Water Practice & Technology

IWA PUBLISHING

Water Practice & Technology Vol 16 No 4, 1078 doi: 10.2166/wpt.2021.067

CuO as efficient photo catalyst for photocatalytic decoloration of wastewater containing Azo dyes

Martha Ramesh
Physics, Humanities and Science, ACE Engineering College, Ankushapure, Ghatkesar, Medchal, Telangana 501301, India
E-mail: ramesh.martha09@gmail.com

MR, 0000-0002-7322-3868

ABSTRACT

Cupric oxide nanoparticles (CuO NPs) were prepared via a chemical precipitation method using the precursor of copper (II) nitrate trihydrate. X-ray diffraction analysis confirms that the CuO NPs were a monoclinic crystal structure. The energy band gap of CuO NPs was found to be about 1.76 eV. The obtained CuO NPs were used as a photo catalyst to decolorize various dyes, such as methylene blue (MB), acid yellow 23 (AY 23) and reactive black 5 (RB 5), with a low concentration in the presence of visible light. The results show that the highest decolorization achieved was 67.8% and 66.3% for RB-5 dye and AY-23 dye, while 43.5% for MB dye from aqueous solution at 5 h illumination. The obtained CuO NPs were used as a photo catalyst to decolorize various dyes, RB-5, AY-23 and MB dye obeys pseudo first order kinetics with values of −0.112, −0.174 and −0.201 h^{-1}, respectively.

Key words: acid yellow 23, CuO NPs, methylene blue, molecular weight, photo decolorization, reactive black 5

HIGHLIGHTS

- Chemically prepared Cupric oxide nanoparticles (CuO NPs) were used as efficient photo catalyst for degrading Azo dyes.
- The energy band gap of CuO NPs was found to be about 1.76 eV.
- Azo dyes like RB-5, AY-23 and MB obey pseudo first order kinetics.
- The photocatalysis results show that the highest degradation achieved was 67.8% and 66.3% for RB-5 dye and AY-23 dye, while 43.5% for MB dye from aqueous solution at 5 h illumination.
- The enhanced photo catalytic degradation of Azo dye can be explained in terms of ion charge and molecular weight.
- Evaluation of photocatalytic degradation of RB5 and MB with reported literature data.

GRAPHICAL ABSTRACT

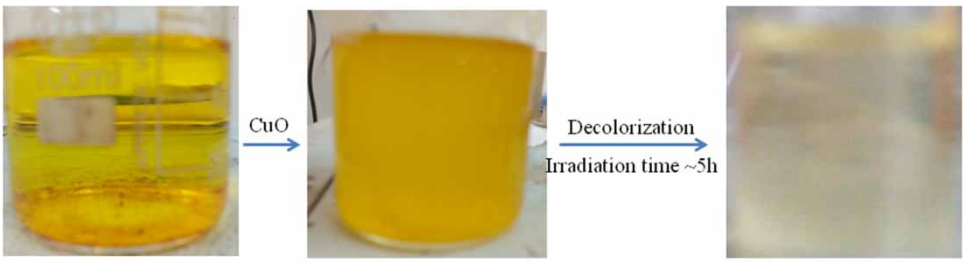

1. INTRODUCTION

The azo dyes are by far the most important class, accounting for over 50% of all commercial dyes, and have been studied more than any other class. Azo dyes are organic compounds bearing the functional group R′-*N* = N-R, in which R′ and R are usually aryl. The azo group is attached to two groups, of which at least one, but more usually both, is aromatic. They exist in the trans form E-*N* = N-A in which the bond angle is ca. 120°, the nitrogen atoms are sp^2 hybridized, and the designation of A and E groups is consistent with C.I. usage (Hunger & Herbst 2007). In which, the E group consists of electron-donating substituents, particularly amino and hydroxyl groups, and the

A group often contains electron-accepting substituents. If the dyes contain only aromatic groups, such as naphthalene and benzene, they are known as carbocyclic azo dyes. If they contain one or more heterocyclic groups, the dyes are known as heterocyclic azo dyes (Abinaya *et al.* 2018).

Azo dyes are normally characterized by color and high levels of chemical oxygen demand (COD) (Xiong *et al.* 2001). Among the Azo dyes, RB 5, AY-23 and MB are widely commercially used due to their high shade of the color, solubility and easy attachment of the fibre. Due to their various usage purposes, viz. protein fiber, synthetic fiber and cellulosic fiber, they are widely used in the textile industry for dyeing. During the dyeing processes, there is always a portion of applied dyes that remains unfixed to the fabrics and is washed out. The unfixed dyes are found to be in high concentrations in textile effluents. Since it is poisonous, corrosive, reactive, acidic, and flammable, it must be processed before being reused or redirected into the water supply. In general, the effluent might contain harmful substances such as heavy metals, toxic chemicals, oil and grease, solids, sludge, organic and inorganic materials. Toxic compounds in the effluent can seriously disrupt humans, animals and the environment as a whole. If a large amount of biodegradable substances end up in the water, organisms can begin to break them down. This is a bad thing because these species absorb a lot of dissolved oxygen as they do so. For marine life to survive, dissolved oxygen is essential. As it becomes depleted, fish can be harmed in life-threatening ways. Other types of waste, like oil and grease, are more difficult to break down and can accumulate on the water's surface. This reduces the amount of light available to photosynthetic aquatic plants. It can also suffocate fish and get caught in birds' feathers. And heavy metals, such as lead and mercury, are harmful not only to humans but also to animals. If someone consumed or ate fish from a polluted water source they might suffer significant health consequences. The same can be said for the animals and plants that live in the water. Further, pouring sludge into waterways before it has been properly handled can have long-term environmental consequences. Dumping sludge may cause water to become warm or even hot. The temperature of the water can increase in these conditions, affecting the amount of oxygen in it. Therefore, for the sake of human and aquatic life, development of cost-effective and eco-friendly treatment is the recent global priority (Selvakumar *et al.* 2013; Abdel *et al.* 2019; Jie *et al.* 2019).

In recent years, a great deal of attention has been dedicated to chemical processes such as Fenton, defoamation and adsorption for decolorization of water pollutants by transition metal oxides catalysts due to low toxigenicity, ideally with CO_2 and H_2O as the end products (Cynthia *et al.* 2020; Mahdieh & Seyed 2020). However, in practical dye wastewater treatment, such treatments still challenge with other disadvantages, such as a slow reaction rate to decolorize effluents, complex chemistry and metal ion sludge.

An alternative to conventional methods, heterogeneous photocatalysis has emerged as a green technology and is most promising because of its complete mineralization of organic pollutants by light irradiation (Fox & Dulay 1993). Nevertheless, the advances in heterogeneous photocatalysis are manipulation of matter or methods at their factual principles are leading to potential solutions for the depollution of water. The widely used metal oxides like TiO_2 (Tao *et al.* 2011), NiO (Harraz *et al.* 2010), MnO_2 (Ramesh *et al.* 2016), WO_3 (Liu *et al.* 2010) and so on have relatively large band gap energies, the photocatalytic efficiencies, which are based on the full UV spectrum, are rather low and unstable. Moreover, a major drawback is that commercial catalysts require potential oxidants and suppress the regeneration of hydroxyl radicals and lower the catalytic activity during the decomposition of H_2O_2 (Kim & Choi 2005). Some of these materials were reported based on artificial UV-light as the energy source. However, UV in natural sunlight represents only 5%-8% of the solar spectrum at sea level and this provides a limitation and the requirement for artificial illumination of the catalysts (Ibhadon & Fitzpatrick 2013). The metal sulfide semiconductors such as CdS and PbS are regarded as insufficiently stable for catalysis and are toxic (Kakodkar n.d.). Recently, heterogeneous nanostructures decorated with BiOCl (Wang *et al.* 2017), C_3N_4 (Wang *et al.* 2015) were reported to show some photo catalytic promise, but with uncertainty over their efficiencies and spectral characteristics.

Besides, heterogeneous photocatalysis deals with the experimental determination and analysis of the concentration of a substance as a function of time. The rate of reaction measured based on the concentration (A) can be given below (Herrmann 1999).

$$r = -d[A]/dt = k[\text{reactant}]^n \quad (1)$$

where k is the rate constant and the power n is the order. A reaction is zero, first, second or third order depending on the value of n (0, 1, 2 or 3 respectively). The parameter k as well can be zero order, first order, second order or third order rate constant. The rate constant can be utilized in comparing the rate of different reactions. Hence, the catalytic efficiency in heterogeneous photocatalysis depends on a variety of environmental conditions such as surface charge

and electronic structure of the catalyst, the nature of the surface-active center, the degree of localization of photo generated charges, pH, temperature, the nature of the pollutant, the crystalline structure, synthesis method and photo reactor dimension.

The copper oxide (CuO) nanostructure has gained significant attention because it is a very reactive, lower band gap semiconductor with monoclinic structure and their high surface volume exhibits remarkable applications in catalysis (Vaseem *et al.* 2008). Moreover, CuO is cheap, abundant, and the economic material with short reaction time under normal conditions is advantageous in green synthesis of nanoparticles. Pan *et al.* fabricated CuO photocatalyst via *Pyrus Pyrifolia* leaf extract method showed the decolorization percentage of methylene blue around 45% at 30 h under visible irradiation (Sundaramurthy & Parthiban 2015). After introduction of chemical reduction, the photocatalytic activity of CuO photocatalyst was almost 82% dye decolorization at the same time under UV light irradiation (Raghav *et al.* 2016), the highest decolorization of MB was recorded 93% at 120 min under heating of 600 °C (sunlight) by electrochemically prepared CuO NPs (Katwal *et al.* 2015). Manjari *et al.* reported that biosynthesized CuO NPs showed 91% conversion efficiency for 6 cycles in the decolorization of methylene blue (Manjari *et al.* 2017). Although the photocatalytic activity of CuO modified by the various methods and laboratory conditions has been improved, the system still suffers from many limitations including high cost and complicated synthesis process, or instability during photochemical operations. Chemical precipitation method of a simple and eco-friendly approach for the synthesis of copper oxide nanoparticles was developed, it highlights the use of chemical entities for the synthesis of copper oxide nanoparticles. For example, Rao *et al.* (2017) prepared the CuO nanostructures using chemical precipitation and reported its efficient photocatalytic activity at about 88% at 4 h towards tartrazine decolorization under visible light illumination. Henceforth, in this perspective, this study focused on chemical precipitation applied in the synthesis of copper oxide nanoparticles, an eco-friendly approach, and evaluated their efficacy for the catalytic reduction of organic dyes, namely RB-5, MB and AY-23, from liquid phases by heterogeneous photocatalysis.

Photo-catalysis may be termed as a photo induced reaction, which is accelerated by the presence of a catalyst. It can be initiated by the absorption of a photon with energy equal to or higher than the catalyst band-gap energy (Eg) (Xu *et al.* 2006). The absorption leads to a charge separation due to the excitation of an electron (e^-) from the valence band of the catalyst to the conduction band, thus creating a hole (h^+) in the valence band (Equation (2)). Due to the generation of electrons and holes, reduction-oxidation reactions take place at the surface of CuO NPs. In the reduction reaction, the conduction band electrons could reduce the dye or react with electron acceptors such as O_2 adsorbed on the Cu(II) surface or dissolved in water, reducing it to superoxide radical anion $O_2^{-\bullet}$ (Equations (3) and (4)). In the oxidation reaction, the valence band holes can oxidize the organic molecule to form R^+, or react with OH^- or H_2O oxidizing them into $OH^\bullet$ radicals (Equations (5)–(7)). Together with other highly oxidant species like peroxide radicals, they are reported to be responsible for the CuO photo decolorization of organic substrates as dyes (Equations (8) and (9)). The resulting $^\bullet OH$ radical (Equations (10) and (11)), being a very strong oxidizing agent, can oxidize most azo dyes to the mineral end-products (Equation (12)). According to this, the relevant reactions at the CuO surface causing the decomposition of dyes can be expressed as follows (Devi & Singh 2014).

$$CuO + h\nu\ (\text{visible}) \rightarrow CuO(e_{CB-} + h_{VB+}) \quad (2)$$

$$CuO(e_{CB-}) + O_2 \rightarrow O_2^{\bullet -} + CuO \quad (3)$$

$$CuO(e_{CB-}) + \text{Dye} \rightarrow \text{reduction products} \quad (4)$$

$$CuO(h_{VB+}) + H_2O \rightarrow CuO + H^+ + OH^- \quad (5)$$

$$CuO\ (h_{VB+}) + OH^- \rightarrow CuO + OH^\bullet \quad (6)$$

$$CuO(h_{VB+}) + \text{Dye} \rightarrow \text{oxidation products} \quad (7)$$

$$O_2^{\bullet -} + H^+ \rightarrow HO_2^\bullet \quad (8)$$

$$HO_2^\bullet + HO_2^\bullet \rightarrow H_2O_2 + O_2 \quad (9)$$

$$H_2O_2 + O_2^{\bullet -} \rightarrow OH^\bullet + OH^- + O_2 \quad (10)$$

$$H_2O_2 + h\nu \rightarrow 2OH^\bullet \quad (11)$$

$$Dye^{\bullet +} + O_2(O_2^\bullet \text{ or } OH^\bullet) \rightarrow \text{decolorized products}* \quad (12)$$

Product*: CO_2, H_2O, mineral acid and nontoxic inorganic compounds.

2. EXPERIMENTAL

2.1. Materials and methods

Reactive black 5 (RB-5), Methylene blue (MB), Acid yellow 23 (AY-23), Copper (II) nitrate trihydrate (Cu $(NO_3)_2.3H_2O$), Sodium dodecyl sulfate (SDS), Potassium hydroxide (KOH), ammonia. All these items were purchased from Sigma-Aldrich and used without purification. Millipore double distilled (DD) water (18.2 MΩ) was used for preparing the solutions. All reactions were conducted with stirring using magnetic stirrer (Remi MLH Plus, India) at 700 rpm and centrifugation was passed out using centrifuge (Remi, R-8C, India).

2.2. Chemical structure of Azo dyes

Figure 1 shows the chemical structure of Azo dyes. Azo dyes contain one, two, three, or more azo linkages; linking phenyl, naphthyl rings usually substituted with some functional groups like triazine amine, chloro, hydroxyl, methyl, nitro, and sulfonate. Figure 1(a) shows the chemical structure of the RB-5, it is an anionic sulfonated diazo reactive dye type and has the molecular formula $Na_4O_{19}S_6C_{26}H_{21}N_5$ with a molar mass of 991.83 g/mol, measurable at a wavelength of 596 nm. It comprises a vinyl sulfone group as the reactive group (a fiber-bonding site of the reactive dye, 'reactive hook'). Due to the relatively high reactivity of the vinyl sulfone group with water (residual moisture, air humidity), RB-5 is present in many commercial products in a protected form. AY-23 is an anionic dye type and has the molecular formula $C_{16}H_9N_4Na_3O_9S_2$ with a molar mass of 534.37 g/mol, measurable at a wavelength of 432 nm. As can be seen in Figure 1(b), AY-23 is synthesized by reaction of sulfanilic acid with 3-carboxy-l-(4-sulfophenyl)-5-pyrazolone. AY-23 consists essentially of 3-corboxy-5-hydroxy-1-(4′-sulphophenyl)-4-(4′-sulphophenylazo) pyrazole trisodium salt and subsidiary coloring matters together with sodium chloride and/or sodium sulphate as the principal uncoloured components. Wherein MB is a thiazine dye (Figure 1(c)), and is a cationic dye type with the molecular formula $C_{16}H_{18}ClN_3S$ with a molar mass of 319.85 g/mol, measureable at a wavelength of 664 nm. MB is a formal derivative of phenothiazine and the hydrated form has 3 molecules of water per unit of methylene blue. When MB is oxidized, it gets serially demethylated and forms all the tri-, di-, mono- and non-methyl intermediates, which are Azure A, Azure B, Azure C, and thionine, respectively.

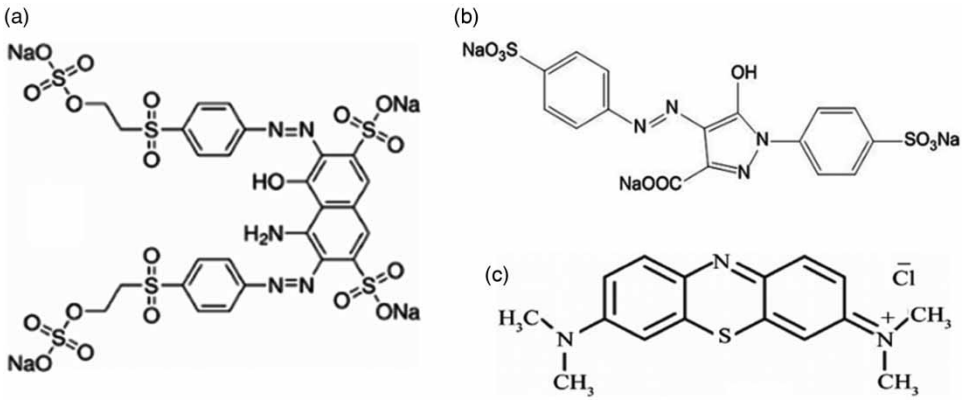

Figure 1 | Shows the chemical structure of (a) RB-5, (b) AY-23 and (c) MB.

CuO NPs have been synthesized by chemical precipitation treatment. In a typical process, 0.5 g of SDS was first added to 100 mL of Cu $(NO_3)_2.3H_2O$ (0.2 M) solution, which was followed by the dropping of 100 mL of 0.4 M KOH under constant stirring until a homogeneous solution was obtained. After being stirred for 30 min, 50 mL of ammonia solution (12.5 wt %, ~7.0 M) was injected slowly and the whole mixture was stirred continuously at ambient temperature for 15 h. The resultant suspension was filtered, washed thoroughly several times with DD water and ethanol in order to remove the surface modifier, and then dried at 80 °C for 12 h in a vacuum. Finally, the as-prepared $Cu(OH)_2$ nanostructures were calcined at 400 °C for 4 h.

The structural analysis of synthesized catalyst was performed using powder X-ray diffraction (Rigaku miniflex 600, Japan) and it was operated at a voltage of 40 kV and a current of 30 mA with Cu Ka (1.5405 Å) radiation in the scanning range from 20 to 80 with a step size of 0.025°. The surface morphology of the synthesized catalyst

was determined by SEM (JEOL/JSM-6380LA, Japan) with a resolution of 20 KV to 1 KV, magnification X50-10,00,000, accelerating range 0.1–30 kV. The optical properties of the catalyst was recorded using a UV-Vis spectrometer (Ocean Optics USB4000-UV-VIS, India) in the spectral range of 400 to 800 nm and distilled water was used as a blank.

2.3. Photocatalysis

The photocatalytic experiments were carried out using RB-5, MB and AY-23 as model dyes and CuO NPs as the photocatalyst under visible irradiation. The visible irradiation was supplied by a tungsten halogen light source (24 V/150 W) with a wavelength ranging between 380–800 nm (Fisher Scientific, Republic of Korea). The reactor consists of a rectangular shaped reaction vessel of size (W × H) of 26 × 41 cm^2. The measured light intensity was 11.9 W/m^2. The irradiation was from above and the distance to the suspension surface was 10 cm. For the reaction, 20 mg of CuO NPs was dispersed in 100 mL of 3×10^{-5} M dye (RB-5 or MB or AY-23) solution at neutral pH, and stirred magnetically with a rate of 600 rpm to maintain homogeneity in the reaction mixture.

The proportion of each dye to the catalyst was considered to be the same or optimal. Conversely, the different amount of dye used on the catalyst gives various turbidity of the suspension, intern, and strongly inhibits similar light penetration in the dye-catalyst system. To continue the catalytic reaction, the reaction mixture was stirred in the dark for 30 min to ensure the proper adsorption-desorption equilibrium of dye molecules on the catalyst surface. Then the visible light was irradiated on the suspension for the whole reaction of 5 h. The samples (5 mL) were withdrawn from the reaction mixture at regular interval of time (1 h for each sample), filtered using a Polyvinylidene difluoride of 0.45 μm and analyzed for the residual dye concentration remaining in the solution by recording the absorption spectra using an Ocean Optics USB4000-UV-VIS spectrophotometer. Actually, all experiments were performed at room temperature.

The decolorization efficiency (%) of dye was determined using the formula, % decolorization = $(C_0 - C_t)/C_0 \times 100$, where C_0 and C_t is the concentration of the initial and extracted solution, respectively (Chen *et al.* 2015).

In addition, the wastewater containing the dye normally contains other additive substances like H_2O_2, and atmospheric super oxide ions usually that are corrosive to the catalyst and damaging to dye. These chemical additives may temporarily be originated into the light affected wastewater, allow chemical agents like OH_2, and O_2 to pass through the photolysis and into the adsorption system. As a result, oxidising agents like $OH^{\bullet}$, $HO_2^{\bullet}$ and $O_2^{\bullet}$ can become suspended in the waste water and transported into the dye molecules, clogging catalyst pores, causing interaction of the dye CuO system with the photons, and affecting CuO photocatalytic efficiency rates (as per Equations (2)–(12)) (Bhaskar *et al.* 2011; Guolin *et al.* 2017).

2.4. Decolorization kinetics

To evaluate the kinetic rate of different dyes' color removal, the obtained experimental data (Figure 5) for various dyes were treated with three kinetic models, the zero order, first order and second order types, which can be described by the following equations (Mukhlish *et al.* 2013).

$$C_t - C_0 = -k_0 t (zero\ order) \tag{13}$$

$$\ln (C_t/C_0) = -k_1 t (First\ order) \tag{14}$$

$$1/C_t = k_2 t\ (second\ order) \tag{15}$$

3. RESULTS AND DISCUSSION

3.1. Structural and optical properties

Figure 2(a) shows the XRD analysis of prepared CuO NPs. All the diffraction peaks were well indexed to the monoclinic phase of CuO (JCPDS card No. 00-002-1041) with lattice constants of a = 4.6500 Å, b = 3.410 Å, c = 5.110 Å and $\alpha = \gamma = 90°$, $\beta = 99°$ (Maddinedi & Mandal 2014). SEM was used to study the morphology of the CuO NPs. It is obvious in Figure 2(b) that the CuO NPs had a spherical shape with smooth surface and connected homogeneous rod-like architecture. It can be seen that the NPs have tens of nanometers in diameter. To study electron transitions in the structure of the CuO NPs, optical absorption spectroscopy was carried out in Figure 2(c). The absorption peak at about 437.6 nm was assigned to the electronic transition from n to π^* molecular orbital's of the ligand, which was good evidence for the presence of CuO NPs. The optical bandgap of

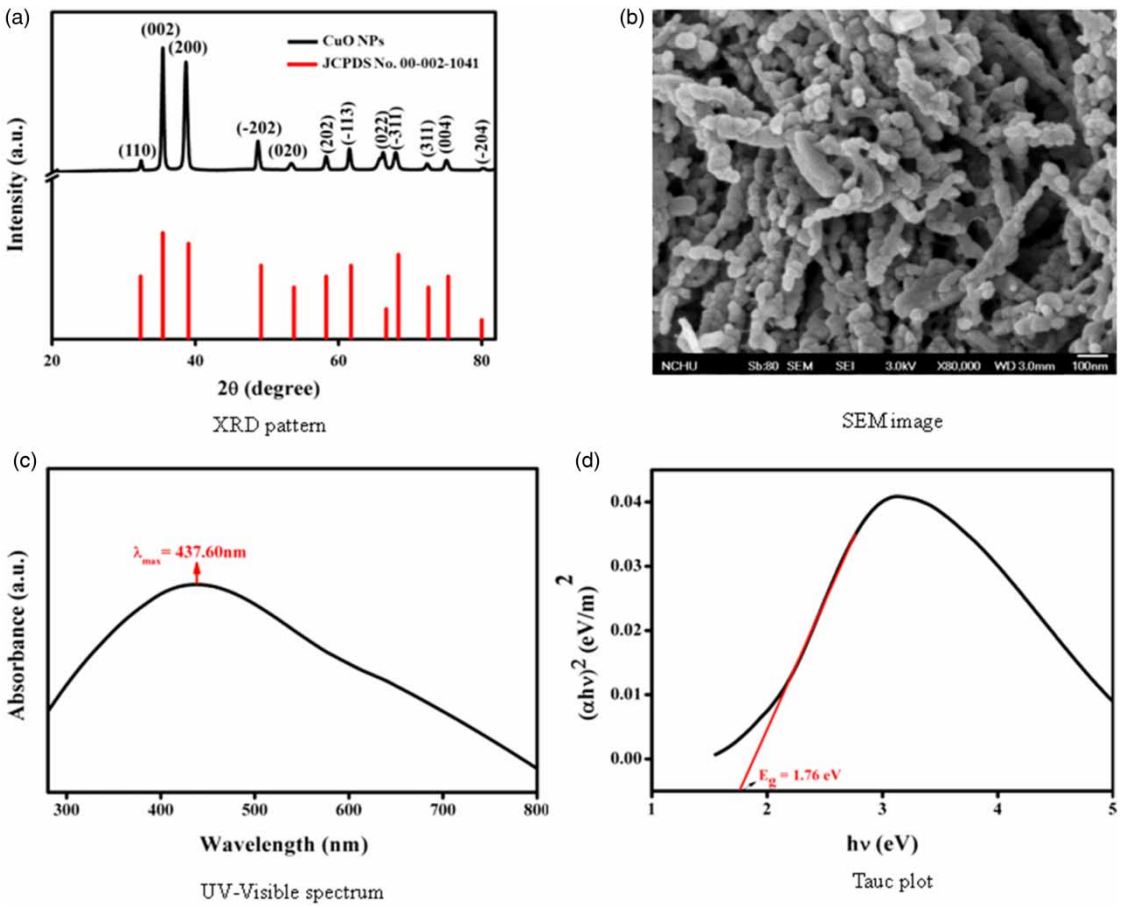

Figure 2 | (a) XRD patterns of CuO nanoparticles prepared in KOH as reducing agent via chemical precipitation process at the 600 rpm stirrer speed and temperature of 400 °C, down graph shows the corresponding JCPDS diffraction pattern of the particles related to the CuO lattice planes, indication the crystalline nature of the CuO nanoparticles, (b) micrograph obtained by SEM shows the spherical nature of as-synthesized of CuO nanoparticles, CuO nanoparticles possess average particle size of 40–60 nm with respect to the bar scale 100 nm at the magnification of ×80 K, (c) UV-Vis the absorption spectrum of CuO nanoparticles by the reaction between 100 mL of 0.4 M KOH and 50 mL of ammonia solution (12.5 wt %, ~7.0 M) under constant stirring for the reaction period of 36 min, CuO NPs show a peak near 438 nm in the wavelength range of 280–800 nm and (d) Tauc plot obtained by plotting the square of the product of the absorption coefficient (proportional to the Kubelka-Munk function) and energy in eV vs. energy. A linear extrapolation provides the bandgap of 1.76 eV for CuO nanoparticles.

CuO NPs was calculated using the Tauc's relation as follows (Bouazizi *et al.* 2015):

$$\alpha h\nu = A(h\nu - E_g)^n \tag{16}$$

where α, ν, A and E_g are the absorption coefficient, light frequency, proportionality constant and band gap energy, respectively. A plot of $(\alpha h\nu)^2$ against photon energy ($h\nu$) (Figure 2(d)) showed a straight line due to direct allowed transition ($n = 1$). The intercept of the straight line corresponds to the optical bandgap (E_g) of CuO NPs, which was estimated to be 1.76 eV.

3.2. Photo catalytic properties of CuO nanoparticles

Figure 3(a) displays the optical (UV-Vis) spectra of dye as a function of irradiation time. There are two major absorption peaks observed, one is in the UV region and the other in the visible region, ascribed to the n – π* and π-π* transitions, respectively. The minor peak that appeared at 250 nm in treated dyes indicates the presence of anthraquinone structure, while the peaks at 281 and 358 nm in RB-5 dye are for vinyl sulphone and benzene, respectively (Laohaprapanon *et al.* 2015). As seen in Figure 3(a), the maximum absorbance was observed at 664, 597 and 442 nm for MB, RB5 and AY-23, respectively, which decreased gradually with exposure time (Laohaprapanon *et al.* 2015).

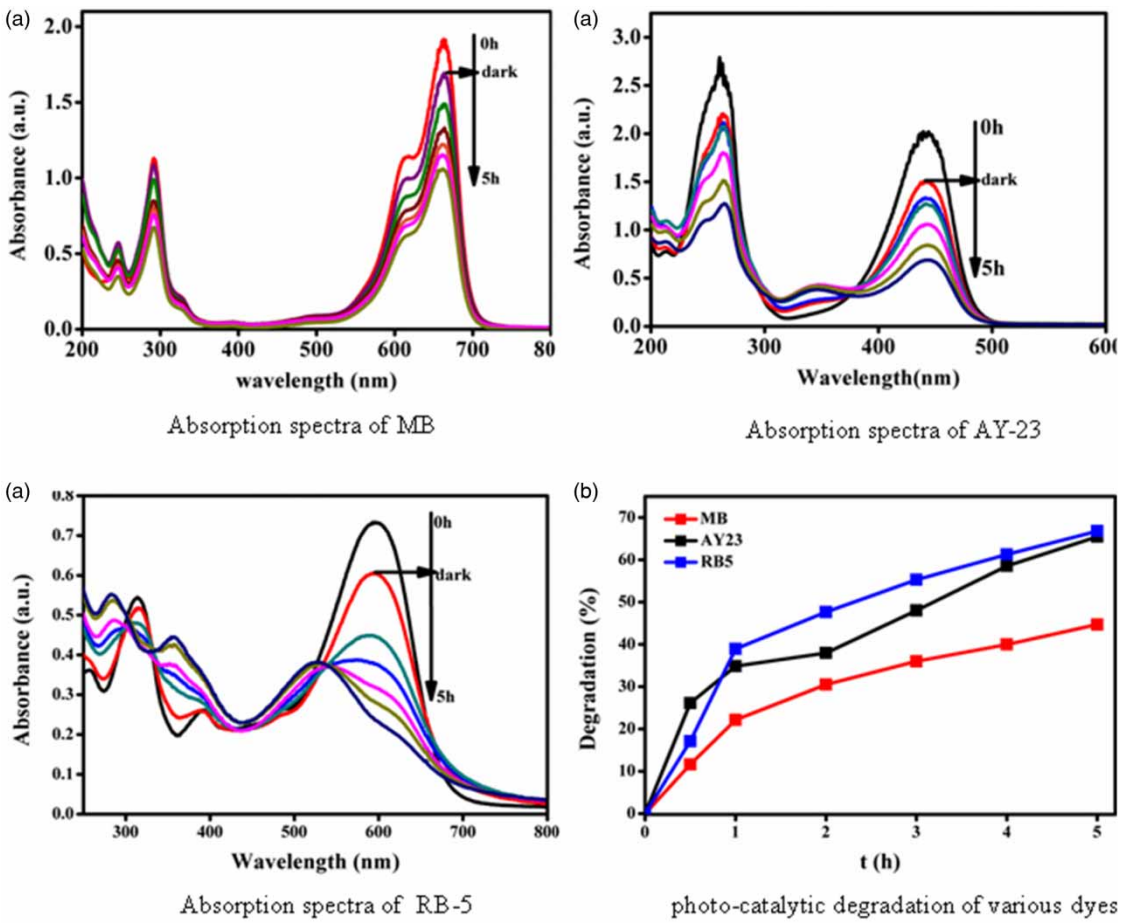

Figure 3 | (a) The UV-Vis spectra for decolorization of the azo dyes under experimental conditions: (MB concentration = 9.59 mg/L, Acid yellow 23 concentration = 16.09 mg/L, RB5 concentration = 29.75 mg/L, CuO dose = 0.2 g/L, time = 5 h, and pH = 7) and (b) the decolorization rate with the photo catalyst CuO under visible light for the azo dyes. It was observed that maximum decolorization 67.8% (RB5) was reported at a CuO dose of 0.2 g/L, followed by 66.3 (AY-23), and 43.5 (MB) at the reaction period of 5 h.

The spectrum at t = 0 is for the starting solution of dye after getting adsorption equilibrium. From the intensity change in the absorption spectra, we can see initially that only a little amount of dye was physically adsorbed by CuO; later, dye concentration quickly decreased. In 60 min, the dye concentration at maximum absorption wavelength (λ_{max}) was reduced by at least one order of magnitude. At the same time, the color of the solution quickly turned from a deep thick color to thin color with respect to the dye (Figure 4). With the further elapse of reaction time, dye absorption peak continually dropped at a slow rate and the original maximum absorption peak was

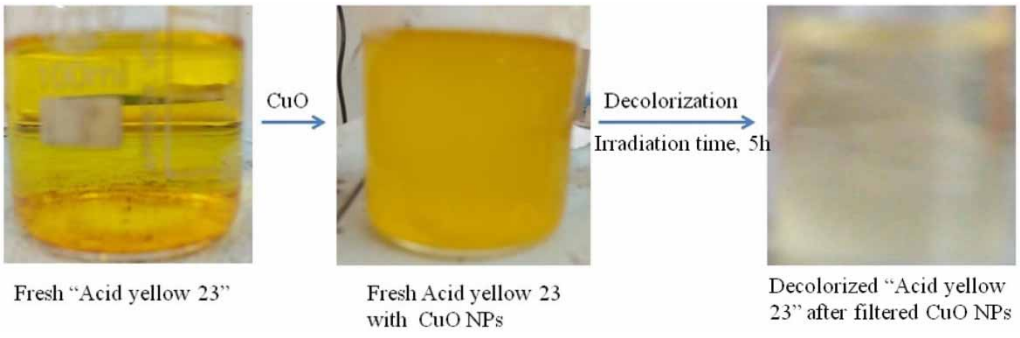

Figure 4 | Shows the decoloriztion test, for the acid yellow 23 as model dye, using 20 mg CuO NPs in the presence of visible light for the irradiation time of 5 h was performed in the laboratory.

noticed to shift slightly towards a lower wavelength, known as blue shift, indicating the catalytic decolorization of dye. Eventually, the band at λ_{max} became very broad and weak, suggesting the complete decolorization of dye. The absorption spectra obtained after complete decolorization suggest that decolorization products are colorless.

Figure 3(b) shows the plot of decolorization efficiency vs. irradiation time for MB, RB-5 and AY-23. The decolorization was 67.8, 66.3 and 43.5% for RB-5, AY-23 and MB dyes, respectively, within 5 h of photo irradiation. According to these results, the photo-catalytic decolorization of RB5 was more compared to the MB and AY-23 because its chemical structure was found to be more favorable for oxidation.

It is assumed that these compounds undergo color change other than the decolorization without the actual breaking apart of the complex dye molecules. More often than not, decolorization occurs when the chromophore bond is broken, but with the major fragments of the original molecule remaining intact. Thus, the disappearance of the color in the wastewater does not mean the degradation of the organic dye molecules. The fact that the organic amines produced under reducing conditions exhibit more toxic effects to the environment than the parent compound is well known.

For comparison, the photocatalytic test of commercial CuO is also investigated using RB-5 dye under the same experimental conditions. The decolorization efficiency of as-synthesized catalyst is found to be higher than the commercial catalyst due to slightly higher Fermi level, higher capacity to adsorb oxygen and higher degree of hydroxylation of the surface act as mentioned worthy reasons for the superior photocatalytic activity of synthesized catalyst than that of commercial catalyst (Tanaka *et al.* 1991). The results found for the CuO are relatively better than the other synthesized catalysts, as shown in Table 1.

Table 1 | Evaluation of photocatalytic decolorization of RB5 and MB with reported literature data

						Photocatalysis			
S.No	Catalyst	Method	Dye	Band gap (eV)	Particle size (nm)	Decolorization (%)	Time (h)	irradiation	References
1	ZnO	*Pyrus Pyrifolia* leaf extract	MB	3.3	22	45	30	Solar	Parthibana & Sundaramurthy (2015)
2	Al-Fe_2O_3	Fluidized-bed reactor	RB5		100	2	1.5	UVA	Hsueh *et al.* (2006)
3	Enterobacter sp. EC3	Phylogenetic	RB5			20	24 dyes	Dark	Wang *et al.* (2009)
4	sunflower seed s		RB5			80	16	Dark	Osma *et al.* (2007)
5	iron(III) oxide	Incipient impregnation	RB5			0	2	Dark	Ersöz (2014)
6	PC500 titania		RB5			60	5	UV	Aguedach *et al.* (2005)
7	CuO/Al_2O_3/ phospahate	Incipient wetness impregnation				35	4	Dark	Bradu *et al.* (2010)
8	NiO/Al_2O_3	Incipient wetness impregnation				50	4	Dark	"
9	$BiVO_4$	Impregnation	MB	2.45	40.2	40	4	Visible	Abdullah *et al.* (2016)
10	CdSe	Hydrothermal	MB	1.76	30	6	4	Visible	Chen *et al.* (2012)
11	Mn_3O_4	Soft template self-assembly	MB		140	1	3	Visible	Zhang *et al.* (2010)
12	CuO	Chemical precipitation	MB RB5	1.76	28.5	43.5 67.8	5 5	Visible Visible	Present Present

The enhanced photo catalytic decolorization of RB-5 can be explained in terms of ion charge and molecular weight. Firstly, based on the ion charge, the variation in photo decolorization is partially caused by the charge variation between MB, AY-23 and RB-5, with MB having a positive charge, and AY-23 and RB-5 having a negative charge. The ion charge will affect the affinity and the adsorption of the dye molecules by the photo catalyst.

Hypothetically, the Cu species will interact with the chitosan matrices through either a Lewis-acid base interaction or hydrogen bonding. Such interaction will cause the Cu in the chitosan matrices to have a positive charge or a neutral one, allowing the positive charge of the surface to have a higher affinity towards electrostatic interaction with anionic dye compared to cationic dye. This will in turn a higher level photo decolorization of anionic dye (Stair 1982). Besides, the electron withdrawal from $NaSO_4$ of the vinylsulphone group in RB-5 makes it as a good electron source than that of the amino group in AY-23 during the light illumination. It means more electrons are available in RB-5 for exciting the conduction band of the catalyst, therefore the more the decolorization efficiency in RB-5.

Secondly, molecular weight plays a crucial role in the dye decolorization efficiency. The molecular weight defines the amount of particles in dye. The more the molecular weight, the more particles are exposed to the photo-catalyst and thus creates a more adsorbed layer over the catalyst surface. According to the second law of photochemistry, each atom or molecule receive one photon; therefore RB-5 receives an excess number of photons compared to AY-23 and MB, in turn increasing the rate of photo catalytic reaction in the system of RB-5-CuO, therefore enhancing the RB-5 decolorization efficiency (Okabe *et al.* 1978).

Reusability is an important parameter to confirm the stability and reproducibility of a photocatalyst. To study the reusability of the catalyst, we collected the catalyst remaining after the decolorization reaction, filtered and dried it, and it was used for further reactions. As shown in Figure 5(a), the as-synthesized CuO photocatalyst was found to be moderately stable up to its fifth cycle. From I-V cycles, the decolorization efficiency decreases only from 67.8 to 63.0%, which is due to the accumulation of byproducts in the cavities of the active surface sites of the catalyst and loss of some amount of catalyst that attaches to the walls of the membrane during the filtering process. Moreover, the stability of the as-synthesized CuO photocatalyst before and after the photocatalytic reaction has also been investigated using XRD analysis, which is shown in Figure 5(b). The XRD results clearly reveal that the CuO NPs are relatively stable and no phase change occurred after five cycles of photocatalytic reaction (Prakash *et al.* 2016). The reusability studies confirmed that the prepared CuO nanostructures are having high photocatalytic stability.

The impact of the photo-catalytic performance on the crystallite parameter of the photo catalyst is also verified in Figure 5(c). Afterwards, we calculated directly values of particle size from peak broadening using the Scherrer formula ($D = (0.9 \times \lambda)/(d \cos\theta)$) and found them to be 75.38 nm before the reaction time and 25.09 nm after the photocatalytic reaction time. After photocatalytic reaction for 5 h, the crystallite size noticeably decreased by approximately 50% due to the formation of secondary grains in the effluent's treated region.

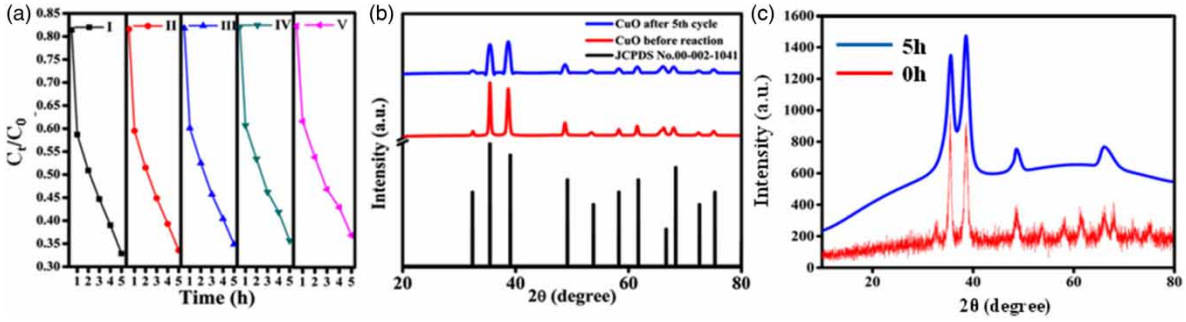

Figure 5 | Reusability of CuO photo catalyst for five successive cycles for the decolorization of RB5. Processing conditions: RB5 concentration = 29.75 mg/L, CuO dose = 0.2 g/ L, PH = 7, visible radiation = 24 V/150 W, time = 5 h, and temperature 30 °C and (b) XRD patterns of CuO nanoparticles before (red spectra) and after photocatalytic decolorization of RB5 for the five cycles (blue spectra), (c) XRD patterns of CuO nanoparticles after photocatalytic decolorization of RB5 for the reaction time of 5 h (blue spectra), indicating the crystalline nature of the CuO nanoparticles.

3.3. Kinetics

The modal kinetic constant (k) and the correlation coefficient (R^2) are shown in Table 2. It was observed that the values of R_1^2 were higher than R_0^2 and R_2^2, confirming that the photo-catalytic decolorization of all dyes on the synthesized CuO NPs can be described by the first order kinetic model (Figure 6). The correlation constant for the fitted line was estimated to be $R_1^2 = 0.993$, 0.992 and 0.981 for RB-5, AY-23 and MB respectively. The

Table 2 | Kinetic parameters for photo catalytic decolorization of MB, AY-23 and RB-5 on CuO NPs

	Zero order		First order		Second order	
Dye	R_0^2	k_0	R_1^2	k_1	R_2^2	k_2
MB	0.960	−0.175	0.981	−0.201	0.890	0.215
AY23	0.973	−0.257	0.992	−0.174	0.926	0.258
RB5	0.981	−0.102	0.993	−0.112	0.953	0.794

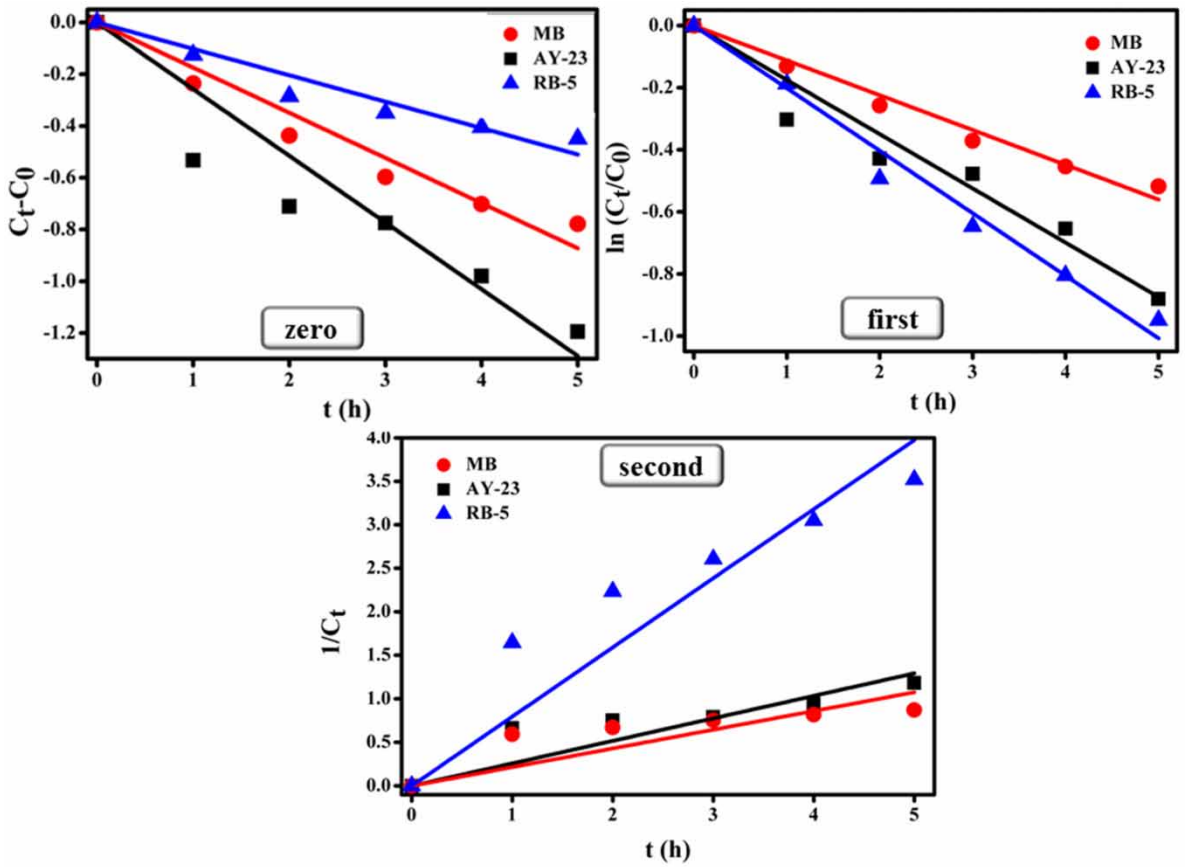

Figure 6 | The effect of CuO nanoparticles on the different dye decolorization plots based on zero order, first order and second order kinetics fitted to the experimental data kinetics for visible illumination, respectively. The obtained CuO NPs were used as a photo catalyst to decolorize various dyes, RB-5, AY-23 and MB dyes obey pseudo first order kinetics with values of −0.112, −0.174 and −0.201 h^{-1} respectively. Processing conditions: MB concentration = 9.59 mg/L, Acid yellow 23 concentration = 16.09 mg/L, RB5 concentration = 29.75 mg/L, CuO dose = 0.2 g/L, time = 5 h, pH = 7, visible radiation = 24 V/150 W and room temperature and pressure.

decolorization reaction rate under the visible light irradiation was found to be $k_1 = -0.112$, −0.174 and −0.201 h^{-1} for the previous dyes, respectively. Among all dyes, the decolorization rate of MB was much lower than the other two dyes. A decrease in the rate constant of MB could be ascribed to the reduced efficiency rate of absorbance of MB in a solution that is reasoned by reduced correspondence to the electron transition in a MB-CuO system (Abdul Rahman *et al.* 2014).

The decolorization rate or kinetic rate constant is also explained in terms of molecular weight of dye. The reaction rate constant quantifies the rate of a chemical reaction, which depends on the mean residence time of the molecule. Mean residence time is that each molecule spends a different amount of time in the chemical reaction. Thus, in knowing the molecular weight, mean residency time is used to estimate the reaction rate constant. According to the results, the reaction rate constant of system RB-5/CuO is much higher than system AY-23/CuO and MB/CuO due to the greater molecular weight of RB-5 compared to the other dyes. The greater the

molecular weight, the more the mean residence time which means molecules of RB-5 last a longer amount of time in the reaction with H_2O/CuO/irradiation. Hence, by increasing the number of events on atomic scale over time, the reaction rate constant increased (Certini *et al.* 2004).

4. CONCLUSION

In this study, CuO NPs were prepared by the chemical precipitation method. CuO NPs were analysed by structural and optical properties. The photo catalytic activities of CuO NPs for decolorization of various organic dyes (RB-5, AY-23, and MB) have been investigated under visible light irradiation. Compared to MB and AY-23, RB5 recorded the highest decolorization, which was around 67.8% at 5 h illumination due to the electrostatic interaction between RB5 and CuO. After a long examination, we can conclude that CuO has a very good potential towards RB5 decolorization under visible light irradiation. Further, kinetic study revealed that the process followed the pseudo first order model for all the dyes. Therefore, it is confirmed that the CuO NPs could be a capable, environmentally benevolent and also cost effective material for water treatment polluted with dye stuff.

ACKNOWLEDGEMENTS

The authors thank the ACE Engineering College for providing all research facilities for this work. We would like to specially thank the Prof. Y. V Gopala Krishnamurthy, general secretary for providing financial support, as well as Mrs M Padmavati, joint secretary and Principal Dr B. L. Raju for encouraging the research work. We greatly appreciate the team of physics branch in ACE Engineering College for their contribution in the moving forward of this research work.

DATA AVAILABILITY STATEMENT

All relevant data are included in the paper or its Supplementary Information.

REFERENCES

Abdel, S., Mansour, H. I. & Sulaiman, A. M. 2019 Anaerobic/aerobic integration via UASB/enhanced aeration for greywater treatment and unrestricted reuse. *Water Practice and Technology* **14**(4), 837–850.

Abdullah, A. H., Peng, W. T. & Hussein, M. Z. 2016 Degradation of methylene blue dye by Cuo-Bivo4 photocatalysts under visible light irradiation. *Malaysian Journal of Analytical Sciences* **20**(6), 1338–1345.

Abdul Rahman, I., Ayob, M. T. M. & Radiman, S. 2014 Enhanced photocatalytic performance of NiO-decorated ZnO nanowhiskers for methylene blue degradation. *Journal of Nanotechnology*. Available from: https://www.hindawi.com/journals/jnt/2014/212694/abs/. Accessed 26 July 2017.

Abinaya, A., Rajib, G. C., Eldhose, I. & Prakash, K. B. G. 2018 Surface modification of date seeds (*Phoenix dactylifera*) using potassium hydroxide for wastewater treatment to remove azo dye. *Water Practice and Technology* **13**(4), 859–870.

Aguedach, A., Brosillon, S., Morvan, J. & Lhadi, E. K. 2005 Photocatalytic degradation of azo-dyes reactive black 5 and reactive yellow 145 in water over a newly deposited titanium dioxide. *Applied Catalysis B: Environmental* **57**(1), 55–62.

Bhaskar, R., Ramachandra, K., Latha, S. S. & Prabhakar, S. 2011 Degradation of dyes by UV/O_3/H_2O_2 and electrooxidation techniques. *Water Practice and Technology* **6**(2), wpt2011038. https://doi.org/10.2166/wpt.2011.038.

Bouazizi, N., Bargougui, R., Oueslati, A. & Benslama, R. 2015 Effect of synthesis time on structural, optical and electrical properties of CuO nanoparticles synthesized by reflux condensation method. *Advanced Materials Letters* **6**(2), 158–164.

Bradu, C., Frunza, L., Mihalche, N., Avramescu, S.-M., Neaţă, M. & Udrea, I. 2010 Removal of reactive black 5 azo dye from aqueous solutions by catalytic oxidation using CuO/Al_2O_3 and NiO/Al_2O_3. *Applied Catalysis B: Environmental* **96**(3), 548–556.

Certini, G., Agnelli, A., Corti, G. & Capperucci, A. 2004 Composition and mean residence time of molecular weight fractions of organic matter extracted from two soils under different forest species. *Biogeochemistry* **71**(3), 299–316.

Chen, M.-L., Meng, Z.-D., Zhu, L., Park, C.-Y., Choi, J.-G., Ghosh, T., Cho, K.-Y. & Oh, W.-C 2012 Synthesis of carbon nanomaterials-CdSe composites and their photocatalytic activity for degradation of methylene blue. *Journal of Nanomaterials* **2012**, 21.

Chen, W., Zheng, L., Jia, R. & Wang, N. 2015 Cloning and expression of a new manganese peroxidase from *Irpex lacteus* F17 and its application in decolorization of reactive black 5. *Process Biochemistry* **50**(11), 1748–1759.

Cynthia, D., Moses, B., Benjamin, I. O., Boredi, S. C., Seteno, K. & Obed, N. 2020 Biofoam formation and defoamation in global wastewater treatment systems. *Water Practice and Technology* **16** (1), 1–18.

Devi, H. S. & Singh, T. D. 2014 Synthesis of copper oxide nanoparticles by a novel method and its application in the degradation of Methyl orange. *Advance in Electronic and Electric Engineering* **4**(1), 83–88.

Ersöz, G. 2014 Fenton-like oxidation of Reactive Black 5 using rice husk ash based catalyst. *Applied Catalysis B: Environmental* **147**, 353–358.

Fox, M. A. & Dulay, M. T. 1993 Heterogeneous photocatalysis. *Chemical Reviews* **93**(1), 341–357.
Guolin, J., Zhengnan, S., Ping, Y., Shirong, W. & Yu, L. 2017 Clays for heterogeneous photocatalytic decolorization of wastewaters contaminated with synthetic dyes: a review. *Water Practice and Technology* **12**(2), 432–443.
Harraz, F. A., Mohamed, R. M., Shawky, A. & Ibrahim, I. A. 2010 Composition and phase control of Ni/NiO nanoparticles for photocatalytic degradation of EDTA. *Journal of Alloys and Compounds* **508**(1), 133–140.
Herrmann, J.-M. 1999 Heterogeneous photocatalysis: fundamentals and applications to the removal of various types of aqueous pollutants. *Catalysis Today* **53**(1), 115–129.
Hsueh, C. L., Huang, Y. H. & Chen, C. Y. 2006 Novel activated alumina-supported iron oxide-composite as a heterogeneous catalyst for photooxidative degradation of Reactive black 5. *Journal of Hazardous Materials* **129**(1), 228–233.
Hunger, K. & Herbst, W. 2007 *Industrial Dyes Chemistry, Properties, Applications*, 3rd edn. Completely Revised Edition, Wiley Frankfurt, Germany. ISBN 3-527-30576-9.
Ibhadon, A. O. & Fitzpatrick, P. 2013 Heterogeneous photocatalysis: recent advances and applications. *Catalysts* **3**(1), 189–218.
Jie, C., Xiaoling, J., Chunxia, Z., Zhe, Q. & Jingfei, W. 2019 Biotoxicity and by-product identification of dye wastewaters. *Water Practice and Technology* **14**(2), 449–456.
Kakodkar, S. B. n.d. *Synthesis, Characterisation and Photocatalytic Activity of Cadmium Sulphide Nanoparticles*. Available from: http://www.e-journals.in/PDF/V5N1/75-78.pdf. Accessed 26 July 2017
Katwal, R., Kaur, H., Sharma, G., Naushad, M. & Pathania, D. 2015 Electrochemical synthesized copper oxide nanoparticles for enhanced photocatalytic and antimicrobial activity. *Journal of Industrial and Engineering Chemistry* **31**, 173–184.
Kim, S. & Choi, W. 2005 Visible-light-induced photocatalytic degradation of 4-chlorophenol and phenolic compounds in aqueous suspension of pure titania: demonstrating the existence of a surface-complex-mediated path. *The Journal of Physical Chemistry B* **109**(11), 5143–5149.
Laohaprapanon, S., Matahum, J., Tayo, L. & You, S.-J. 2015 Photodegradation of reactive black 5 in a ZnO/UV slurry membrane reactor. *Journal of the Taiwan Institute of Chemical Engineers* **49**, 136–141.
Liu, Y., Ohko, Y., Zhang, R., Yang, Y. & Zhang, Z. 2010 Degradation of malachite Green on Pd/WO 3 photocatalysts under simulated solar light. *Journal of Hazardous Materials* **184**(1), 386–391.
Maddinedi, S. B. & Mandal, B. K. 2014 Peroxidase like activity of quinic acid stabilized copper oxide nanosheets. *Austin Journal of Analytical and Pharmaceutical Chemistry* **1**(2), 4.
Mahdieh, R. & Seyed, A. M. 2020 A global trend of Fenton-based AOPs focused on wastewater treatment: a bibliometric and visualization analysis. *Water Practice and Technology* **16** (1), 19–34.
Manjari, G., Saran, S., Arun, T., Rao, A. V. B. & Devipriya, S. P. 2017 Catalytic and recyclability properties of phytogenic copper oxide nanoparticles derived from *Aglaia elaeagnoidea* flower extract. *Journal of Saudi Chemical Society*. Available from: http://www.sciencedirect.com/science/article/pii/S1319610317300352. Accessed 26 July 2017
Mukhlish, M. B., Najnin, F., Rahman, M. M. & Uddin, M. J. 2013 Photocatalytic degradation of different dyes using TiO2 with high surface area: a kinetic study. *Journal of Scientific Research* **5**(2), 301–314.
Okabe, H. others 1978 *Photochemistry of Small Molecules*, Vol. 431. Wiley, New York, NY. Available from: http://www.ans.org/pubs/journals/download/a_17080. Accessed 26 July 2017
Osma, J. F., Saravia, V., Toca-Herrera, J. L. & Couto, S. R. 2007 Sunflower seed shells: a novel and effective low-cost adsorbent for the removal of the diazo dye Reactive Black 5 from aqueous solutions. *Journal of Hazardous Materials* **147**(3), 900–905.
Parthibana, C. & Sundaramurthy, N. 2015 Biosynthesis, characterization of ZnO nanoparticles by using *Pyrus pyrifolia* leaf extract and their photocatalytic activity. *International Journal of Innovative Research in Science, Engineering and Technology* **4**(10), 9710–9718.
Prakash, K., Senthil Kumar, P., Pandiaraj, S., Saravanakumar, K. & Karuthapandian, S. 2016 Controllable synthesis of SnO_2 photocatalyst with superior photocatalytic activity for the degradation of methylene blue dye solution. *Journal of Experimental Nanoscience* **11**(14), 1138–1155.
Raghav, R., Aggarwal, P. & Srivastava, S. 2016 Tailoring oxides of copper-Cu_2O and CuO nanoparticles and evaluation of organic dyes degradation. In: *AIP Conference Proceedings*, Vol. 1724. AIP Publishing, p. 020078. Available from: http://aip.scitation.org/doi/abs/10.1063/1.4945198. Accessed 26 July 2017
Ramesh, M., Nagaraja, H. S., Rao, M. P., Anandan, S. & Huang, N. M. 2016 Fabrication, characterization and catalytic activity of α-MnO_2 nanowires for dye degradation of Reactive black 5. *Materials Letters* **172**, 85–89.
Rao, M. P., Wu, J. J., Asiri, A. M. & Anandan, S. 2017 Photocatalytic degradation of tartrazine dye using CuO straw-sheaf-like nanostructures. *Water Science and Technology* **75**(6), 1421–1430.
Selvakumar, S., Manivasagan, R. & Chinnappan, K. 2013 Biodegradation and decolourization of textile dye wastewater using *Ganoderma lucidum*. *3 Biotech* **3**(1), 71–79.
Stair, P. C. 1982 The concept of Lewis acids and bases applied to surfaces. *Journal of the American Chemical Society* **104**(15), 4044–4052.
Sundaramurthy, N. & Parthiban, C. 2015 Biosynthesis of copper oxide nanoparticles using *Pyrus pyrifolia* leaf extract and evolve the catalytic activity. *International Research Journal of Engineering and Technology* **2**, 332–337.
Tanaka, K., Capule, M. F. & Hisanaga, T. 1991 Effect of crystallinity of TiO_2 on its photocatalytic action. *Chemical Physics Letters* **187**(1–2), 73–76.
Tao, J., Luttrell, T. & Batzill, M. 2011 A two-dimensional phase of TiO_2 with a reduced bandgap. *Nature Chemistry* **3**(4), 296–300.

Vaseem, M., Umar, A., Hahn, Y. B., Kim, D. H., Lee, K. S., Jang, J. S. & Lee, J. S. 2008 Flower-shaped CuO nanostructures: structural, photocatalytic and XANES studies. *Catalysis Communications* **10**(1), 11–16.

Wang, H., Zheng, X.-W., Su, J.-Q., Tian, Y., Xiong, X.-J. & Zheng, T.-L. 2009 Biological decolorization of the reactive dyes Reactive Black 5 by a novel isolated bacterial strain Enterobacter sp. EC3. *Journal of Hazardous Materials* **171**(1), 654–659.

Wang, H., Yuan, X., Wu, Y., Zeng, G., Chen, X., Leng, L. & Li, H. 2015 Synthesis and applications of novel graphitic carbon nitride/metal-organic frameworks mesoporous photocatalyst for dyes removal. *Applied Catalysis B: Environmental* **174**, 445–454.

Wang, H., Yuan, X., Wu, Y., Zeng, G., Tu, W., Sheng, C., Deng, Y., Chen, F. & Wei, C. J. 2017 Plasmonic Bi nanoparticles and BiOCl sheets as cocatalyst deposited on perovskite-type ZnSn (OH) 6 microparticle with facet-oriented polyhedron for improved visible-light-driven photocatalysis. *Applied Catalysis B: Environmental* **209**, 543–553.

Xiong, Y. A., Strunk, P. J., Xia, H., Zhu, X. & Karlsson, H. T. 2001 Treatment of dye wastewater containing Acid orange II using a cell with three-phase three-dimensional electrode. *Water Research* **35**(17), 4226–4230.

Xu, Y., Chen, H., Zeng, Z. & Lei, B. 2006 Investigation on mechanism of photocatalytic activity enhancement of nanometer cerium-doped titania. *Applied Surface Science* **252**(24), 8565–8570.

Zhang, P., Zhan, Y., Cai, B., Hao, C., Wang, J., Liu, C., Meng, Z., Yin, Z. & Chen, Q. 2010 Shape-controlled synthesis of Mn_3O_4 nanocrystals and their catalysis of the degradation of Methylene blue. *Nano Research* **3**(4), 235–243.

First received 4 May 2020; accepted in revised form 27 June 2021. Available online 8 July 2021